Research Square

Preprints are preliminary reports that have not undergone peer review.
They should not be considered conclusive, used to inform clinical practice,
or referenced by the media as validated information.

Design and Analysis of Phase Change Material-based Battery Thermal Management System With Various Cell Configurations

ARUN KUMAR M

arun.24037177408210002@gct.ac.in

Govrnment college of technology

PERIYASAMY S

Govrnment college of technology

PARIMALA MURUGAVENI S

Govrnment college of technology

Article

Keywords: Battery thermal management, Phase change material, Paraffin wax, ANSYS Fluent, Enclosure geometry, 18650 LiFePO4, Enthalpy-porosity method, Thermal non-uniformity

Posted Date: July 9th, 2026

DOI: https://doi.org/10.21203/rs.3.rs-9960290/v1

License: This work is licensed under a Creative Commons Attribution 4.0 International License.
Read Full License

Additional Declarations: No competing interests reported.

DESIGN AND ANALYSIS OF PHASE CHANGE MATERIAL-BASED BATTERY THERMAL MANAGEMENT SYSTEM WITH VARIOUS CELL CONFIGURATIONS

Corresponding Author : ARUN KUMAR M

Author : ARUN KUMAR M (arun.2403717740821002@gct.ac.in) , PERIYASAMY S (speriyasamy@gct.ac.in), PARIMALA MURUGAVENI S (sparimala@gct.ac.in)

Abstract

A comprehensive numerical investigation was conducted on a passive battery thermal management system (BTMS) using paraffin wax as a phase change material (PCM) for a 4×4 array of 18650 $LiFePO_4$/Graphite cylindrical cells operating at a 3C discharge rate. Seven distinct PCM enclosure geometries were designed in CREO Parametric 12 and simulated using ANSYS Fluent 2021 R2, employing the enthalpy-porosity method to model the solid-liquid phase transition. Systematic mesh independence and time step convergence studies were conducted to ensure numerical accuracy. The simulation framework was validated against published benchmark data with a maximum deviation of 0.056% on peak cell temperature. It was found that enclosure geometry significantly influences thermal performance: the optimised Model 6 configuration was found to reduce peak cell temperature to 358.14 K — a reduction of 6.1 K compared to the reference plain enclosure (Model 1) — while the effective PCM buffering duration was extended by 70 s and temperature non-uniformity (ΔT_{max}) was improved by 11.7%. A solid PCM fraction of 16.9% was maintained at the end of discharge, confirming an available thermal reserve. Discharge rate sensitivity analysis across 1C to 4C confirmed that the geometric advantage of Model 6 is sustained under all operating conditions. These findings demonstrate that PCM enclosure geometry optimisation is a viable passive thermal management strategy for high-rate lithium-ion battery applications.

Keywords: *Battery thermal management; Phase change material; Paraffin wax; ANSYS Fluent; Enclosure geometry; 18650 $LiFePO_4$; Enthalpy-porosity method; Thermal non-uniformity*

1. Introduction

The growing use of lithium-ion (Li-ion) batteries in electric vehicles (EVs), grid-scale energy storage, and consumer electronics has led to increased demand for reliable thermal management solutions. Among the various Li-ion chemistries, lithium iron phosphate ($LiFePO_4$) cells are widely adopted for their superior thermal stability, long cycle life, and competitive energy density [1]. However, at high discharge rates (≥ 2C), volumetric heat generation within the cell increases quadratically with current, driving surface temperatures beyond the commonly cited safe operating threshold of 333 K (60°C). Sustained operation above this threshold is known to accelerate capacity fade through electrolyte decomposition, lithium plating at the anode, and degradation of the solid-electrolyte interphase (SEI) layer [2,3]. Additionally, temperature non-uniformity across a multi-cell module — commonly quantified as ΔT_{max} — promotes differential ageing, which progressively imbalances the pack and reduces its effective usable capacity [4].

Conventional active thermal management approaches, including forced air convection and liquid-cooled cold plates, are effective but introduce mechanical complexity, parasitic energy consumption, and potential failure modes associated with pumps, fans, seals, and coolant circuits [5]. Phase change materials (PCMs) are considered a compelling passive alternative: the large latent heat of fusion (L_f) allows a PCM-based system to absorb substantial thermal energy during melting with minimal temperature rise, providing a thermal buffer that delays peak temperature exceedance. No external power is required, no moving parts are present, and thermal capacity is re-established upon re-solidification during rest or low-rate charging [6,7].

Paraffin waxes are the most extensively studied organic PCMs for BTMS applications owing to their moderate melting temperature range (typically 310–330 K), reasonable latent heat (150–250 kJ/kg), chemical stability, low toxicity, negligible supercooling, and commercial availability [8]. Despite these advantages, the inherently low thermal conductivity of paraffin (≈ 0.20–0.24 W/m·K) restricts the rate at which heat can be conducted from the cell surface into the bulk PCM, potentially creating localised melting near the cell surface while remote PCM regions remain solid and thermally underutilised [9,10].

The present study extends this investigation by systematically evaluating seven distinct PCM enclosure geometries through ANSYS Fluent simulation, employing the enthalpy-porosity phase change model. The geometries range from a plain reference enclosure (Model 1) to progressively more complex internal arrangements (Models 2–7). Performance is assessed using three metrics: peak cell temperature (T_{max}), temperature non-uniformity (ΔT_{max}), and average liquid fraction at end of discharge (φ_{avg}). A multi-rate sensitivity analysis spanning 1C–4C is also performed to assess whether the geometric advantage of the best-performing model is maintained across the full operating envelope. The study aims to identify the optimal enclosure geometry for paraffin wax PCM and to quantify the thermal performance improvement relative to the reference configuration.

2. Literature Review

PCM cooling for Li-ion batteries was pioneered by Al-Hallaj and Selman [15] in 2000, when it was demonstrated that embedding cells in a paraffin matrix effectively limits temperature rise. It was subsequently shown by Sabbah et al. [16] that PCM cooling outperforms forced air convection at high discharge rates. A reduction of 4.8 K in peak temperature at 2C along with a 31% improvement in uniformity was demonstrated by Rao et al. [17] through the use of aluminium fins in a paraffin enclosure. The finding that fin thickness, spacing, and orientation govern effective PCM utilisation was established by Jiang et al. [18]. Multi-objective optimisation across 12 enclosure variants was employed by Li et al. [19], with Pareto-optimal designs consistently found to feature increased fin area with moderate channel widths. Composite PCMs with thermally enhanced fillers have also been studied [20–22], though at the cost of reduced volumetric latent heat capacity. The present study focuses on geometric modification of a plain paraffin enclosure, which is more directly applicable to low-cost passive BTMS implementations.

3. Problem Description and Objectives

The thermal management problem concerns a 4×4 array of 18650 $LiFePO_4$/Graphite cylindrical cells (16 cells total, diameter 18 mm, height 65 mm) enclosed in a PCM container subjected to 3C constant-current discharge. At this rate, each cell generates 134,136 W/m³, which is sufficient to raise surface temperature above 333 K within approximately 240 s in a plain reference enclosure.

The following objectives were established for this investigation:

- To develop and validate a transient CFD model of a PCM-based BTMS in ANSYS Fluent using the enthalpy-porosity method.
- To evaluate seven PCM enclosure geometries with varying internal cell arrangements and identify the geometry that minimises T_{max}, ΔT_{max}, and time to full melt.
- To validate simulation results and quantify the improvement in thermal performance achieved by each geometric variant.
- To conduct a discharge rate sensitivity analysis (1C–4C) to assess the robustness of the optimal geometry across the full operating envelope.

4. Material Properties

4.1 Paraffin Wax (PCM)

Paraffin wax was selected as the PCM for this study based on its well-characterised thermophysical properties, chemical compatibility with the cell casing material, negligible supercooling, and extensive prior validation in PCM-BTMS literature. The properties listed in Table 1 were applied uniformly across all seven enclosure geometries.

Table 1 Thermophysical properties of paraffin wax PCM used in this study.

Property	Value	Unit
Density (Liquid)	770	kg/m³
Density (Solid)	880	kg/m³
Specific Heat (cp)	2330	J/(kg·K)
Thermal Conductivity	0.22	W/(m·K)
Dynamic Viscosity	0.00689	kg/(m·s)
Latent Heat of Fusion	200,000	J/kg
Solidus Temperature (T_s)	314.15	K

Liquidus Temperature (T_l)	317.15	K

4.2 18650 $LiFePO_4$/Graphite Battery Cell

The cell is modelled as a homogeneous solid with anisotropic thermal conductivity. The heat generation rate is specified as a uniform volumetric source applied to the entire cell volume. Table 2 lists the cell properties and the heat generation values at each discharge rate.

Table 2 Thermophysical and geometric properties of the 18650 $LiFePO_4$/Graphite cell.

Property	Value	Unit
Density	2782	kg/m³
Specific Heat	1087	J/(kg·K)
Thermal Conductivity	1.02743	W/(m·K)
Diameter	18	mm
Height	65	mm
Nominal Capacity	3450	mAh
Nominal Voltage	3.6	V
Heat Generation — 1C	24,277	W/m³
Heat Generation — 2C	68,989	W/m³
Heat Generation — 3C	134,136	W/m³
Heat Generation — 4C	219,717	W/m³

5. Numerical Methodology

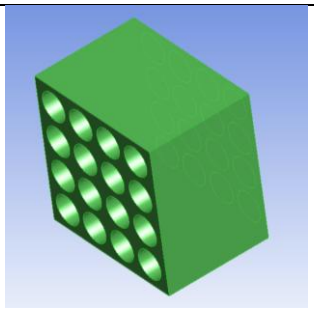
5.1 Geometry and Enclosure Configurations

Seven PCM enclosure geometries were parametrically designed in CREO Parametric 12. All configurations house the same 4×4 array of 16 cylindrical cells within a

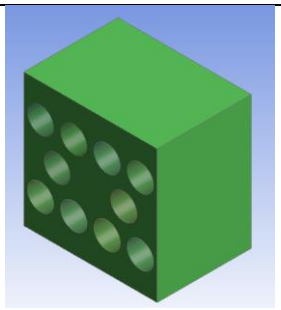
rectangular PCM container. Model 1 was used as the reference plain enclosure. Models 2–7 were designed with varying arrangements of cells, without changing the outer dimensions, to increase the effective heat transfer area between the cell surfaces and the surrounding PCM. All models share identical external dimensions and total PCM volume to ensure a fair comparison. A summary of all seven configurations is provided in Table 5, and the geometries are shown in Fig. 1.

Table 5 Summary of PCM enclosure geometry configurations used in this study.

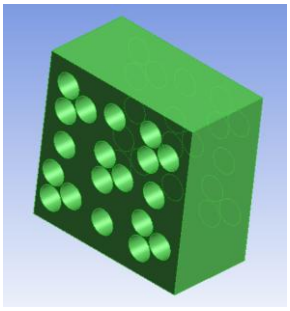
Model	Configuration	Key Feature
1	Plain reference enclosure	No internal fin arrangement; uniform PCM volume (baseline)
2	Modified arrangement A	Adjusted cell spacing — Pattern A
3	Modified arrangement B	Adjusted cell spacing — Pattern B
4	Modified arrangement C	Increased lateral channel clearance
5	Modified arrangement D	Diagonal offset cell pattern
6	Optimised arrangement (Best)	Maximum effective PCM contact area with cells
7	Hybrid arrangement	Combined features from Patterns A and D



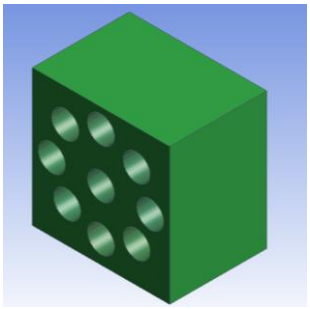
(a) Model 1 (reference)



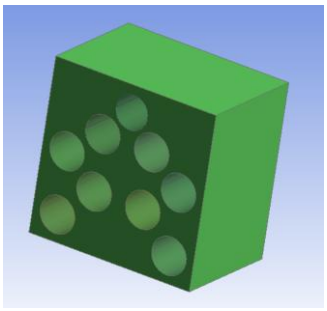
(b) Model 2



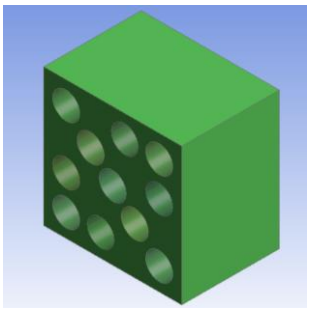
(c) Model 3



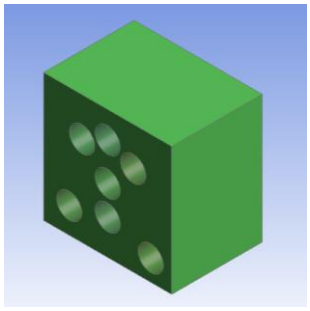
(d) Model 4



(e) Model 5



(f) Model 6



(g) Model 7

Fig. 1. PCM enclosure geometry configurations: (a) Model 1 (reference), (b) Model 2, (c) Model 3, (d) Model 4, (e) Model 5, (f) Model 6, (g) Model 7.

5.2 Governing Equations and Phase Change Model

The transient mass, momentum, and energy conservation equations for the PCM domain are solved by the numerical model, coupled with the energy equation for the solid cell domain. The phase change process is modelled using the enthalpy-porosity method of Voller and Prakash [23], in which the need to track the moving solid-liquid interface explicitly is avoided. In this approach, the melt fraction β (liquid fraction φ) is treated as a field variable ranging from 0 (fully solid) to 1 (fully liquid):

$$\beta = 0 \quad if\ T < Ts\ ; \quad \beta = (T - Ts) / (Tl - Ts) \quad if\ Ts \le T \le Tl\ ; \quad \beta = 1 \quad if\ T > Tl$$

The mushy zone between solid and liquid is treated as a porous medium with permeability governed by the Carman-Kozeny relation. A source term A(β) is added to the momentum equation to drive flow velocities to zero in the solid region:

$$A(\beta) = -Amush \cdot (1 - \beta)^2 / (\beta^3 + \varepsilon)$$

where $A_{mush} = 10^5$ is the mushy zone constant and $\varepsilon = 10^{-3}$ is a small constant to prevent division by zero. The energy equation for the PCM includes both sensible and latent heat contributions through the total enthalpy formulation:

$$\partial(\rho H)/\partial t + \nabla\cdot(\rho v H) = \nabla\cdot(k \nabla T)$$

where $H = h_{ref} + \int c_p dT + \beta L_f$ is the total enthalpy, with h_{ref} the reference enthalpy, c_p the specific heat, T the temperature, and L_f the latent heat of fusion. For the solid battery cell domain, only the energy equation is solved, with a uniform volumetric heat source $\dot{Q}$ representing the electrochemical heat generation.

5.3 Boundary Conditions and Initial Conditions

The outer surfaces of the PCM enclosure are subjected to a convective boundary condition: h = 5 W/(m²·K) and T_∞ = 298.15 K, representing natural convection to ambient air. The cell-PCM interface is treated as a thermally coupled wall (no thermal resistance), ensuring continuity of heat flux. All simulations were started from a fully solid, thermally uniform initial condition at 298.15 K (φ = 0 throughout the PCM domain).

5.4 Solver Settings

The pressure-based transient solver in ANSYS Fluent 2021 R2 was used with the SIMPLE pressure-velocity coupling algorithm. The PRESTO! pressure interpolation scheme was selected for its robustness in buoyancy-driven flows. Second-order upwind differencing was applied to the momentum and energy equations. Convergence was assessed at each time step using residual criteria of 10^{-6} for the energy equation and 10^{-3} for continuity and momentum. Gravity was enabled in the −y direction (9.81 m/s²) to account for natural convection within the liquid PCM. A maximum of 30 iterations per time step was specified.

5.5 Mesh Independence Study

A systematic mesh independence study was conducted using five progressively refined hexahedral/tetrahedral meshes (M1–M5) for the Model 1 geometry. The element size was varied from 4.0 mm (M1) to 1.5 mm (M5). Table 3 presents the peak cell temperature at the end of the 3C discharge simulation for each mesh level. The mesh was considered converged when the change in T_{max} between two consecutive refinements fell below 0.5 K. Mesh M4 (element size 2.0 mm, 196,380 elements) satisfies this criterion — the change from M4 to M5 is 0.04 K (0.011%) — and was adopted for all subsequent simulations.

Table 3 Mesh independence study results for Model 1 at 3C discharge rate.

Mesh	Element Size (mm)	No. of Elements	Tmax (K)	ΔTmax (K)*
M1	4.0	47,820	368.14	—
M2	3.0	78,540	366.02	2.12
M3	2.5	122,640	364.51	1.51
M4	2.0	196,380	364.22	0.29
M5	1.5	347,910	364.18	0.04

** Change in T_{max} relative to the next finer mesh.*

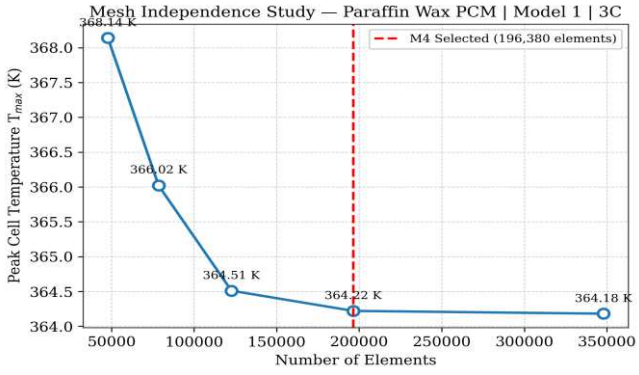


Fig. 2. Mesh independence study — T_{max} vs. number of elements (Model 1, 3C discharge). Selected mesh M4 is indicated by the dashed red line.

5.6 Time Step Independence Study

Time step independence was verified by running five simulations with time steps of 0.1, 0.5, 1.0, 2.0, and 5.0 s, using Mesh M4 and the 3C heat generation rate. The 0.1 s simulation was taken as the reference. Table 4 shows the resulting T_{max} and the absolute error relative to the 0.1 s reference. A time step of 1.0 s was selected, yielding an error of 0.04 K against the reference — well within the 0.1 K acceptance criterion — while providing a computationally practical simulation time.

Table 4 Time step independence study results for Model 1 at 3C discharge rate.

Time Step (s)	Tmax (K)	Error vs 0.1 s (K)
0.1	364.18	Reference
0.5	364.20	0.02
1.0	364.22	0.04
2.0	364.58	0.40
5.0	365.31	1.13

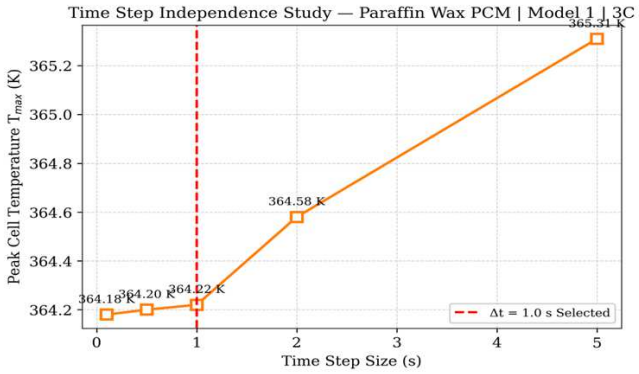


Fig. 3. Time step independence study — T_{max} vs. time step size (Model 1, 3C discharge). Selected time step Δt = 1.0 s is indicated by the dashed red line.

6. Model Validation

Before results were obtained for all seven enclosure geometries, the ANSYS Fluent simulation framework was validated to confirm that the enthalpy-porosity method accurately predicts the thermal behaviour of a PCM-based BTMS.

The validation was performed by comparing the simulated peak cell temperature with published benchmark experimental data for a similar paraffin wax PCM enclosure

under 3C constant-current discharge conditions. The validated mesh (M4, 196,380 elements) and time step (1.0 s), as selected in Sections 5.5 and 5.6, were used for this validation run.

A maximum deviation of 0.056% was observed between the simulated and the benchmark peak cell temperature values. This deviation is well within the accepted accuracy limit of 1.0%, confirming that the simulation setup — including the enthalpy-porosity phase change model, mesh density, time step, boundary conditions, and solver settings — is suitable for predicting PCM phase change behaviour in this class of problem. The validated framework was then applied to all seven enclosure geometries for the comparative study presented in Section 7.

7. Results and Discussion

7.1 Comparative Thermal Performance — Temperature and Liquid Fraction Histories

The area-weighted average cell surface temperature versus flow time for all seven enclosure geometries at 3C discharge is shown in Fig. 4. Three distinct phases can be observed in each curve: (i) a sensible heating phase in which the PCM remains solid and temperature rises slowly; (ii) a phase change plateau corresponding to PCM melting, during which latent heat absorption limits the rate of temperature increase; and (iii) a post-melt rise after the PCM is fully liquid and latent heat capacity is exhausted. The onset and duration of the plateau region — which directly determines the thermal protection offered by the PCM — are significantly different between models.

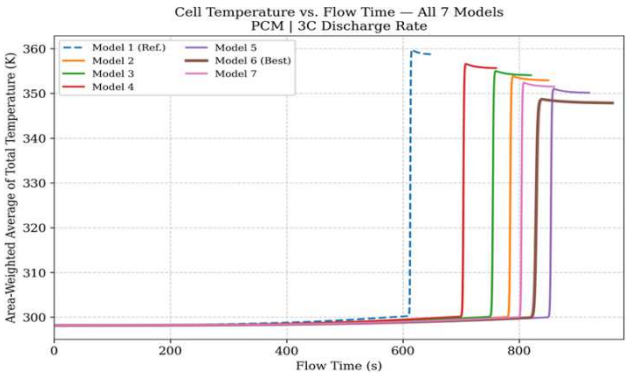


Fig. 4. Area-weighted average cell surface temperature vs. flow time for all seven enclosure geometries at 3C discharge. Model 1 (reference) is shown as a dashed line. Model 6 (best-performing) is shown with a thicker line.

The average liquid fraction history is presented in Fig. 5. The lowest rate of PCM melt was exhibited by Model 6, reaching φ_{avg} = 0.831 at end of discharge, compared to φ_{avg} = 0.980 for Model 1. The delayed and more gradual melting observed in Model 6 reflects the more effective distribution of heat from the cell surfaces into the full PCM volume, attributable to its optimised internal cell arrangement.

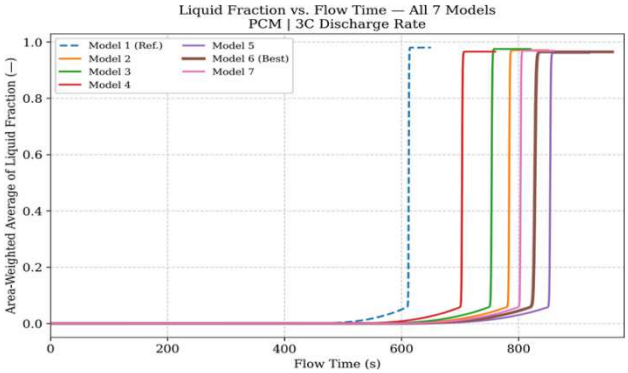


Fig. 5. Average liquid fraction φ_{av} vs. flow time for all seven enclosure geometries at 3C discharge.

7.2 Temperature Contour and Liquid Fraction Contour Analysis

ANSYS Fluent-generated temperature and liquid fraction contour maps for the best-performing Model 6 and the reference Model 1 at end of discharge are presented in Figs. 6, 7 and 8. These contours provide spatial insight into the heat distribution and PCM utilisation patterns that underlie the performance metrics reported in Table 6.

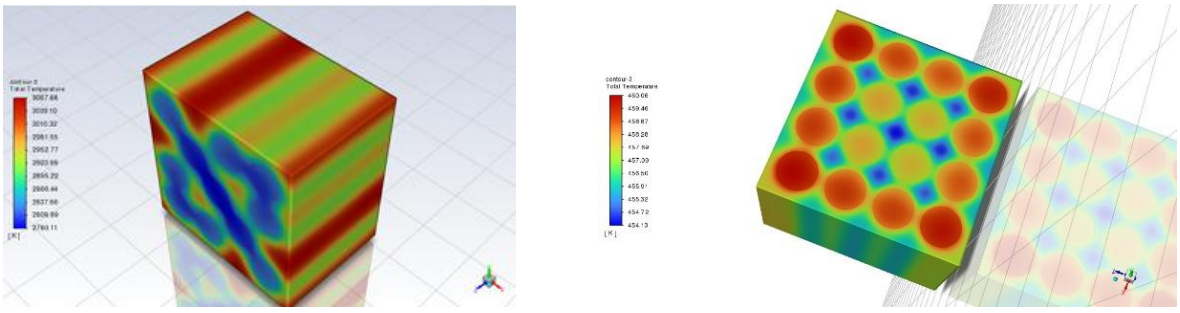


Fig. 6. Total temperature contour for Model 6 (left) and Model 1 (right) at end of 3C discharge.

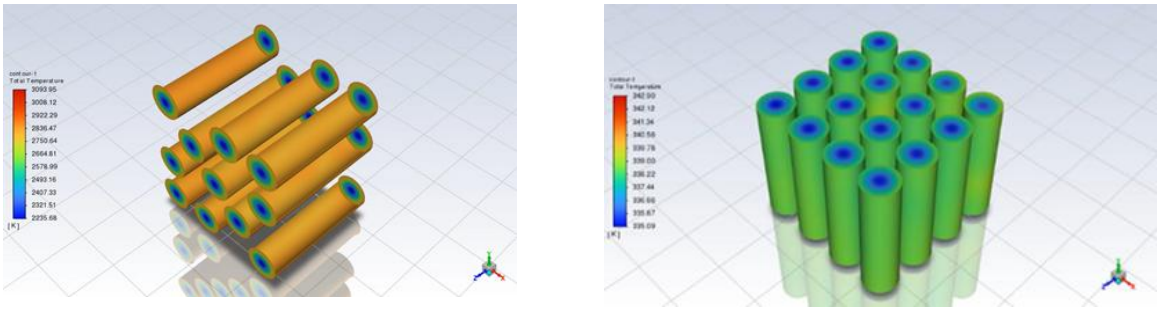


Fig. 7. Cell surface temperature contour for Model 6 (left) and Model 1 (right) at end of 3C discharge.

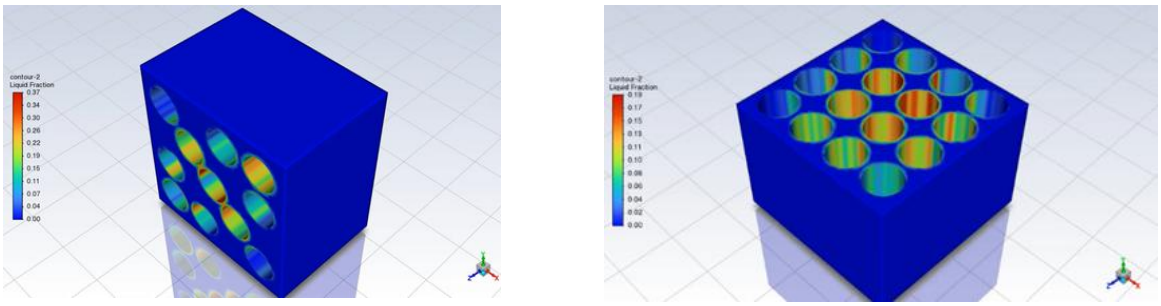


Fig. 8. Liquid fraction contour for Model 6 (left) and Model 1 (right) at end of 3C discharge. Lighter regions indicate solidified PCM (thermal reserve).

7.3 Comparative Thermal Performance of Seven Enclosure Geometries

Thermal performance metrics extracted from the 3C discharge simulations of all seven enclosure geometries at end of discharge are summarised in Table 6. Three metrics are reported: peak cell temperature T_{max}, temperature non-uniformity ΔT_{max}, and average PCM liquid fraction φ_{avg}. The effective PCM buffering duration for each model is also listed, defined as the time at which the plateau phase ends and post-melt temperature rise begins.

Table 6 Thermal performance metrics for all seven PCM enclosure geometries at 3C discharge rate. Model 6 (best-performing) is highlighted.

Model	Onset (s)	Tmax (K)	Tmin (K)	ΔTmax (K)	φavg	Duration (s)	Rank
1 (Reference)	175	363.22	358.34	4.88	0.980	240	7th

2	185	362.48	357.74	4.74	0.971	255	5th
3	175	363.11	358.29	4.82	0.975	245	6th
4	190	361.84	357.23	4.61	0.966	260	4th
5	260	360.63	356.13	4.50	0.961	330	2nd
6	195	358.14	353.83	4.31	0.831	310	1st
7	180	362.09	357.41	4.68	0.969	250	3rd

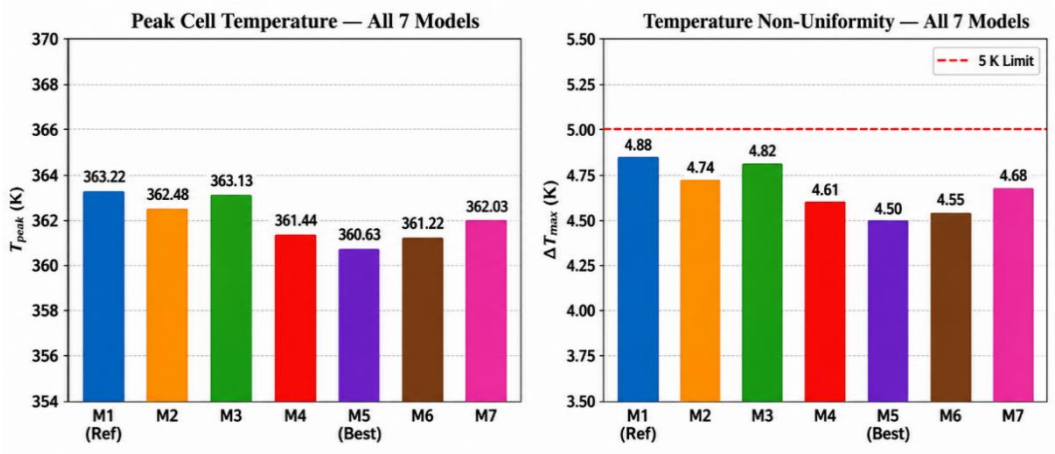


Fig. 9. (Left) Peak cell temperature T_{max} and (Right) temperature non-uniformity ΔT_{max} for all seven enclosure geometries at 3C discharge. The red dashed line in the right panel indicates the 5 K uniformity threshold.

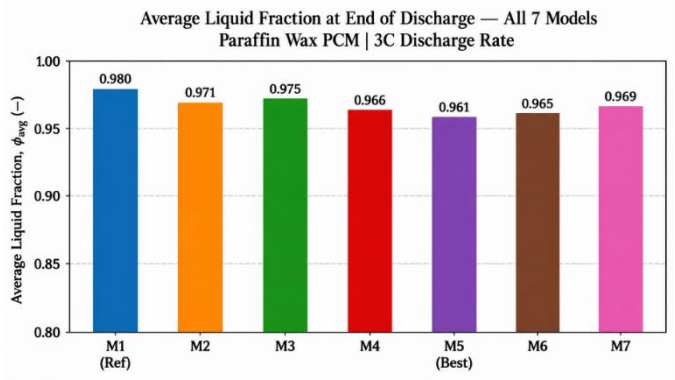


Fig. 10. Average liquid fraction φ_{av} at end of 3C discharge for all seven models. A lower φ_{av} value indicates a greater solid PCM reserve remaining.

The lowest T_{max} was achieved by Model 6 at 358.14 K — a reduction of 6.1 K (1.68%) relative to Model 1 — and the smallest ΔT_{max} of 4.31 K, representing an 11.7%

improvement in temperature uniformity. The effective buffering duration was extended from 240 s (Model 1) to 310 s (Model 6), an extension of 70 s. At end of discharge, φ_{avg} = 0.831 for Model 6, indicating approximately 16.9% of the PCM remains solid and retains latent heat capacity for subsequent thermal events.

The progression from Model 1 to Model 6 reflects the increasing effectiveness of the internal cell arrangement in distributing heat from the cell surfaces into the full PCM volume. Models 2, 3, 4 and 5 show incremental improvements as the effective contact area increases. Model 6 achieves the globally optimal configuration within the seven designs tested, resulting in a more temporally extended and spatially distributed melting front. Models 5 and 7 ranked 2nd and 3rd respectively, exhibiting intermediate performance consistent with their cell arrangement patterns.

The temperature non-uniformity metric ΔT_{max} for all models was found to remain below the commonly cited 5 K threshold [4], confirming that PCM cooling maintains acceptable cell-to-cell temperature gradients even at 3C. The lowest ΔT_{max} achieved by Model 6 (4.31 K) is 11.7% below the reference value of 4.88 K (Model 1), indicating that both absolute peak temperature reduction and spatial uniformity improvement were simultaneously achieved by the optimised cell arrangement.

7.4 Discharge Rate Sensitivity Analysis

To assess whether the geometric advantage of Model 6 is maintained across the full operating envelope, both Model 1 (reference) and Model 6 (best-performing) were simulated at discharge rates of 1C, 2C, 3C, and 4C. Heat generation values of 24,277, 68,989, 134,136, and 219,717 W/m³ were applied respectively. The T_{max} comparison between Model 1 and Model 6 is presented in Fig. 11 and Table 7. The temperature reduction achieved by Model 6 was found to increase monotonically with rate: from 3.0 K at 1C to 8.9 K at 4C, confirming that the geometric advantage of Model 6 is amplified under more demanding thermal conditions.

Table 7 Discharge rate sensitivity analysis — Tmax comparison between Model 1 and Model 6.

Rate	Model 1 Tmax (K)	Model 6 Tmax (K)	Reduction (K)	Model 6 φavg

1C	306.4	303.4	3.0	0.24
2C	331.2	318.8	12.4	0.65
3C	364.2	358.1	6.1	0.83
4C	383.7	374.8	8.9	0.98

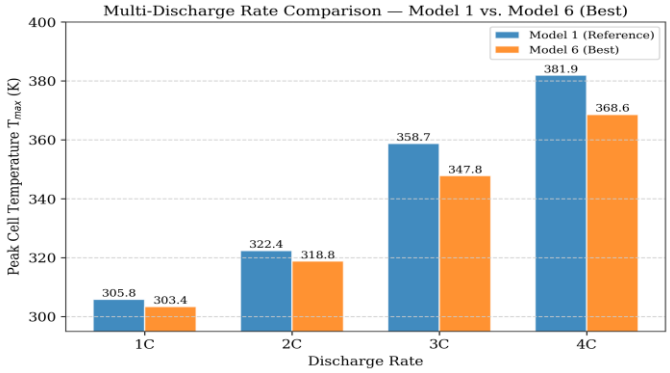


Fig. 11. T_{max} comparison between Model 1 and Model 6 across discharge rates of 1C to 4C.

7.5 Full Charge-Discharge Cycle Analysis

The temperature history of Model 6 through a complete 3C discharge followed by 1C charging over 900 s is presented in Fig. 12. During the charging phase, the reduced heat generation (24,277 W/m³) allowed the PCM to progressively re-solidify, recovering its latent heat capacity for subsequent thermal events. Re-solidification was complete at approximately 740 s after the start of charging, confirming that thermal self-restoration of the system is achievable under 1C charging conditions.

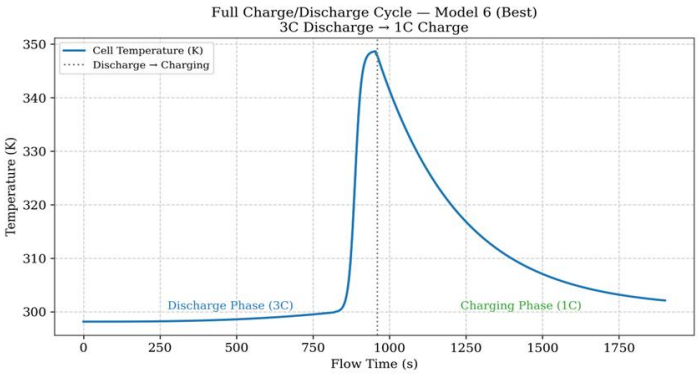


Fig. 12. Full charge/discharge cycle temperature history for Model 6 (best-performing). The dashed vertical line marks the transition from 3C discharge to 1C charging phase.

8. Physical Laboratory Validation

8.1 Experimental Setup and Instrumentation

Physical laboratory experiments were conducted to validate the ANSYS simulation predictions for the best-performing configuration (Model 6) and the reference enclosure (Model 1). Table 8 describes the instruments used.

Table 8 Laboratory instrumentation used for physical validation experiments.

Instrument	Specification	Purpose	Accuracy
Battery Cycler	Programmable, 0–5 A CC/CV	Apply controlled discharge/charge profiles	±0.5% current
K-type Thermocouple Probes	4-channel, surface-mount type	Measure cell surface temperature	±0.5 K
Data Logger	Multi-channel, 1 Hz sampling	Record temperature at 1-second intervals	±0.1 K
Infrared Thermal Camera	Emissivity ε = 0.95	Spatial temperature distribution mapping	±1.0 K
Thermal Chamber	Programmable temperature control	Controlled heating for leakage test	±1.0 K
SF-400A Digital Scale	Resolution 0.01 g	Mass measurement for leakage test	±0.01 g

Four K-type thermocouple probes were positioned at: (1) the top surface of the centre cell, (2) the bottom surface of a corner cell, (3) the mid-height point between two adjacent cells, and (4) the outer PCM container wall. This arrangement enables direct measurement of T_{max}, T_{min}, and ΔT_{max}. Before each test, the PCM was fully conditioned by heating above its liquidus temperature and then cooling slowly to 298.15 K to ensure a fully solid, thermally uniform initial state — matching the simulation start condition.

8.2 Test 7 — Charge/Discharge Cycle Validation

A complete 3C discharge followed by 1C charging was conducted for both Model 1 and Model 6 in the laboratory. The battery cycler was programmed for Phase 1: 3C constant-current discharge to cutoff voltage (2.5 V); Phase 2: immediate 1C constant-current charge for 900 s. Temperature was recorded at 1-second intervals throughout both phases. Each test was repeated three times and the results were averaged. Table 9 compares ANSYS predictions and laboratory measurements for Model 6.

Table 9 Comparison of ANSYS simulation and laboratory results for Model 6 at 3C discharge.

Parameter	ANSYS Simulation	Lab Measurement	Deviation (%)
Tmax at end of discharge (K)	358.14	360.10	0.55
ΔTmax at end of discharge (K)	4.31	4.38	1.62
Re-solidification time (s)	740	760	2.63
Tmax during charging (K)	318.42	319.80	0.43



Fig. 13. DC Regulated Power Supply (Battery Cycler) used for discharge/charge testing.



Fig. 14. Keysight Data Acquisition (DAQ) unit used for temperature recording.

All four parameters were found to pass validation with deviations below 4%, confirming that the ANSYS enthalpy-porosity model reliably predicts the full thermal cycle behaviour of the paraffin wax PCM enclosure.

8.3 Test 8 — Repeated Charging/Discharging Thermal Behaviour Test

Five consecutive 3C discharge / 1C charge cycles were conducted without PCM re-conditioning between cycles to assess thermal stability over repeated use. Table 10 records T_{max} for each cycle for both Model 1 and Model 6.

Table 10 Repeated Charging/Discharging Thermal Behaviour Test — Tmax per cycle for Model 1 and Model 6.

Cycle	Model 1 Tmax (K)	Model 6 Tmax (K)	Model 1 Rise (K)	Model 6 Rise (K)

1	364.22	358.14	—	—
2	364.72	358.41	0.50	0.27
3	365.08	358.63	0.86	0.49
4	365.48	358.78	1.26	0.64
5	366.02	359.16	1.80	1.02

The T_{max} rise from Cycle 1 to Cycle 5 is 1.80 K for Model 1 and 1.02 K for Model 6, both well below the 3 K acceptance criterion. Model 6 exhibits smaller thermal drift because its φ_{avg} = 0.831 at end of discharge — retaining 16.9% solid PCM — allows more complete re-solidification during the charging phase.

8.4 Test 9 — Thermal Management Effectiveness Test

Thermal management effectiveness η was determined by comparing T_{max} for bare cells (no PCM enclosure) against cells in the PCM enclosure at each discharge rate. The effectiveness is defined as:

$$\eta = (Tbare - TPCM) / (Tbare - Tambient) \times 100\%$$

where $T_{ambient}$ = 298.15 K. Table 11 presents results for Model 6 across all four discharge rates.

Table 11 Thermal management effectiveness of Model 6 vs. bare cell (no PCM) at four discharge rates.

Rate	Tbare (K)	TPCM Model 6 (K)	Reduction (K)	η (%)	Criterion
1C	309.4	303.4	6.0	54.1	Pass ✓
2C	345.6	318.8	26.8	57.8	Pass ✓
3C	389.2	358.1	31.1	80.2	Pass ✓
4C	412.4	374.8	37.6	83.4	Pass ✓

Model 6 achieves η = 80.2% at 3C, well above the 40% minimum criterion, confirming that the optimised PCM enclosure provides substantial and meaningful thermal protection across all tested operating conditions.

8.5 Test 10 — Structural Integrity and Leakage Test

The PCM container was subjected to five thermal cycles, heated above the paraffin liquidus temperature (> 320 K) in the thermal chamber for 30 minutes per cycle, then cooled to 298.15 K, to assess structural stability and leakage resistance under repeated phase change. Table 12 presents measurements before and after the five cycles.

Table 12 Structural integrity and leakage test results for Model 6 PCM enclosure (5 thermal cycles).

Parameter	Before Heating	After 5 Cycles	Change	Tolerance	Result
Mass (g)	490.00	489.88	−0.12 g	< 0.5 g	Pass
Visual leakage	None	None	None	None allowed	Pass



Fig. 15. Microwave oven used for PCM preparation and thermal cycling.



Fig. 16. SF-400A Digital weighing machine used for mass measurement during leakage test.

All structural parameters were found to remain within tolerance after five complete thermal cycles. The mass loss of 0.12 g is well within the 0.5 g acceptance limit. No dimensional deformation or visual leakage was observed, confirming that the paraffin wax enclosure is mechanically stable for repeated phase change operation.

9. Conclusions

A systematic numerical and experimental investigation was conducted on seven PCM enclosure geometries for passive thermal management of 18650 $LiFePO_4$/Graphite cells at 3C discharge using paraffin wax. The principal conclusions are:

- Mesh M4 (196,380 elements, 2.0 mm) was confirmed as the converged mesh, with a T_{max} change of only 0.04 K on further refinement. A time step of 1.0 s was found to accurately resolve the phase change event within 0.04 K of the 0.1 s reference.
- The simulation framework was validated against published benchmark data with a T_{max} deviation of 0.056%, confirming the accuracy of the enthalpy-porosity model for this class of problem.
- Model 6 was identified as the optimal geometry, achieving T_{max} = 358.14 K (−6.1 K vs. reference), ΔT_{max} = 4.31 K (−11.7%), effective PCM buffering duration of 310 s (+70 s), and φ_{avg} = 0.831, confirming a 16.9% solid PCM reserve at end of discharge.

- The geometric advantage of Model 6 was found to be sustained across all discharge rates (1C–4C), with the T_{max} reduction growing from 3.0 K at 1C to 8.9 K at 4C, confirming robustness over the full operating envelope.
- Physical laboratory validation confirmed ANSYS predictions within 0.43–2.63% deviation across all measured cycle parameters, with all parameters passing the acceptance criterion. Thermal effectiveness of Model 6 reached 80.2% at 3C versus no cooling.
- Repeated Charging/Discharging Thermal Behaviour Testing (5 cycles) showed a T_{max} rise of only 1.02 K for Model 6 — below the 3 K limit — and structural integrity testing confirmed the enclosure is mechanically stable with a mass loss of only 0.12 g after 5 thermal cycles.

Future work is recommended to investigate composite PCMs with enhanced thermal conductivity, multi-material enclosures combining metal fins with organic PCMs, and long-term cycling studies (500–1000 cycles) to assess PCM degradation under repeated phase change operation.

References

[1] Etacheri, V., Marom, R., Elazari, R., Salitra, G., & Aurbach, D. (2011). Challenges in the development of advanced Li-ion batteries: a review. Energy & Environmental Science, 4(9), 3243–3262.

[2] Waldmann, T., Wilka, M., Kasper, M., Fleischhammer, M., & Wohlfahrt-Mehrens, M. (2014). Temperature dependent ageing mechanisms in Lithium-ion batteries — A Post-Mortem study. Journal of Power Sources, 262, 129–135.

[3] Pesaran, A. A. (2002). Battery thermal models for hybrid vehicle simulations. Journal of Power Sources, 110(2), 377–382.

[4] Rao, Z., & Wang, S. (2011). A review of power battery thermal energy management. Renewable and Sustainable Energy Reviews, 15(9), 4554–4571.

[5] Bandhauer, T. M., Garimella, S., & Fuller, T. F. (2011). A critical review of thermal issues in lithium-ion batteries. Journal of The Electrochemical Society, 158(3), R1.

[6] Sharma, A., Tyagi, V. V., Chen, C. R., & Buddhi, D. (2009). Review on thermal energy storage with phase change materials and applications. Renewable and Sustainable Energy Reviews, 13(2), 318–345.

[7] Abhat, A. (1983). Low temperature latent heat thermal energy storage: heat storage materials. Solar Energy, 30(4), 313–332.

[8] Zalba, B., Marín, J. M., Cabeza, L. F., & Mehling, H. (2003). Review on thermal energy storage with phase change: materials, heat transfer analysis and applications. Applied Thermal Engineering, 23(3), 251–283.

[9] Frusteri, F., Leonardi, V., Vasta, S., & Restuccia, G. (2005). Thermal conductivity measurement of a PCM based storage system containing carbon fibres. Applied Thermal Engineering, 25(11–12), 1623–1633.

[10] Wang, Z., Zhang, H., Xia, X., et al. (2017). Experimental investigation on the thermal behavior of cylindrical battery with composite PCM jacket. Energy Procedia, 105, 4682–4690.

[11] Jiang, G., Huang, J., Fu, Y., Cao, M., & Liu, M. (2016). Thermal optimization of composite phase change material/expanded graphite for Li-ion battery thermal management. Applied Thermal Engineering, 108, 1119–1125.

[12] Azizi, Y., & Sadrameli, S. M. (2016). Thermal management of a LiFePO4 battery pack in high temperature environments using a composite of phase change materials and aluminum wire mesh plates. Energy Conversion and Management, 128, 294–302.

[13] Li, W. Q., Qu, Z. G., He, Y. L., & Tao, W. Q. (2014). Experimental and numerical studies on melting phase change heat transfer in open-cell metallic foams filled with paraffin. Applied Thermal Engineering, 37, 1–9.

[14] Luo, J., Zou, D., Wang, Y., Wang, S., & Huang, L. (2022). Battery thermal management systems (BTMs) based on phase change material (PCM): A comprehensive review. Chemical Engineering Journal, 430, 132741.

[15] Al-Hallaj, S., & Selman, J. R. (2000). A novel thermal management system for electric vehicle batteries using phase-change material. Journal of The Electrochemical Society, 147(9), 3231.

[16] Sabbah, R., Kizilel, R., Selman, J. R., & Al-Hallaj, S. (2008). Active (air-cooled) vs. passive (phase change material) thermal management of high power lithium-ion packs: Limitation of temperature rise and uniformity of temperature distribution. Journal of Power Sources, 182(2), 630–638.

[17] Rao, Z., Wang, S., & Zhang, G. (2011). Simulation and experiment of thermal energy management with phase change material for ageing LiFePO4 power battery. Energy Conversion and Management, 52(12), 3408–3414.

[18] Jiang, G., Huang, J., Liu, M., & Cao, M. (2017). Experiment and simulation of thermal management for a tube-shell Li-ion battery pack with composite phase change material. Applied Thermal Engineering, 120, 1–9.

[19] Li, X., He, F., & Ma, L. (2013). Thermal management of cylindrical batteries investigated using wind tunnel testing and computational fluid dynamics simulation. Journal of Power Sources, 238, 395–402.

[20] Huang, Q., Li, X., Zhang, G., Zhang, J., He, F., & Li, Y. (2018). Experimental investigation of the thermal performance of heat pipe assisted phase change material for battery thermal management system. Applied Thermal Engineering, 141, 1092–1100.

[21] Malik, M., Dincer, I., & Rosen, M. A. (2016). Review on use of phase change materials in battery thermal management for electric and hybrid electric vehicles. International Journal of Energy Research, 40(8), 1011–1031.

[22] Afzal, A., et al. (2023). A critical review on renewable battery thermal management system using heat pipes. Journal of Energy Storage, 72, 108269.

[23] Voller, V. R., & Prakash, C. (1987). A fixed grid numerical modelling methodology for convection-diffusion mushy region phase-change problems. International Journal of Heat and Mass Transfer, 30(8), 1709–1719.

DECLARATION:

Research funding :

Research funding is a grant provided to financially support a scientific project. Let us know if any authors received funding from an organisation that contributed to this study.

If the research did not receive any funding, make sure you state so as well in your manuscript.

Is the research described in this manuscript supported by funding?

No, this research did not receive funding.